pISSN 2384-1095
eISSN 2384-1109

iMRI 2021;25:266-280

https://doi.org/10.13104/imri.2021.25.4.266

iMRI
Investigative Magnetic Resonance Imaging

Radiomics and Deep Learning in Brain Metastases: Current Trends and Roadmap to Future Applications

Yae Won Park[1], Narae Lee[2], Sung Soo Ahn[1*], Jong Hee Chang[1], Seung-Koo Lee[1]

[1]Yonsei University College of Medicine, Seoul, Korea
[2]Wonju Severance Christian Hospital, Yonsei University Wonju College of Medicine, Wonju, Korea

Advances in radiomics and deep learning (DL) hold great potential to be at the forefront of precision medicine for the treatment of patients with brain metastases. Radiomics and DL can aid clinical decision-making by enabling accurate diagnosis, facilitating the identification of molecular markers, providing accurate prognoses, and monitoring treatment response. In this review, we summarize the clinical background, unmet needs, and current state of research of radiomics and DL for the treatment of brain metastases. The promises, pitfalls, and future roadmap of radiomics and DL in brain metastases are addressed as well.

Keywords: Artificial intelligence; Brain metastases; Deep learning; Machine learning; Radiomics

Review Article

Received: February 8, 2021
Revised: May 3, 2021
Accepted: May 3, 2021

Correspondence to:
Sung Soo Ahn, M.D., Ph.D.
Yonsei University College of Medicine, 50-1 Yonsei-ro, Seodaemun-gu, Seoul 03722, Korea.
Tel. +82-2-2228-7400
Fax. +82-2-393-3035
E-mail: sungsoo@yuhs.ac

INTRODUCTION

Brain metastases are the most common type of intracranial tumours in adults; they occur in 20-40% of patients with systemic cancer and are a major cause of morbidity and mortality. Majority of brain metastases occur in patients with primary lung, breast, and colorectal cancers, as well as in those with melanoma or renal cell carcinoma (1). For managing patients with brain metastases, early and accurate diagnosis using magnetic resonance imaging (MRI) is crucial for determining potential treatment strategies. Various treatment approaches such as surgical resection, stereotactic radiosurgery (SRS), whole brain radiation therapy (WBRT), targeted molecular therapy, and immunotherapy, have all been shown to increase survival in eligible patients compared to those who go untreated (2-5). In recent years, treatment professionals have overcome previous scepticism as it relates to the management of patients with brain metastases, which was formerly considered a single disease with a uniform outcome; it is now well recognized that the prognosis for patients with brain metastases is vastly heterogeneous. In the Graded Prognostic Assessment (GPA) (6), a graded prognostic index for patients with brain metastases, the number of brain metastases is included as a prognostic factor in primary lung cancer, melanoma, and renal cell cancer, reflecting the pivotal role of imaging in determining prognosis.

In this era of precision medicine, brain metastases should be accurately detected, segmented, and identified according to their molecular markers, prognosis, and response to treatment. Advances in artificial intelligence technologies have led to the gradual

conversion of medical images into high-dimensional data appropriate for data mining and data science techniques. Radiomics and deep learning (DL) expands the role of imaging in the assessment of brain metastases beyond traditional visual image analysis performed by radiologists by performing laborious tasks such as brain metastases detection and segmentation, and obtaining additional diagnostic and prognostic information from images.

In this article, we aim to review current radiomics and DL research as they relate to brain metastases and provide a roadmap for future applications. Additionally, because we consider the clinical purpose of radiomics and DL as important as the cutting-edge technique itself, we also briefly introduce the clinical background and unmet clinical needs in each section.

Brief Introduction of Radiomics and DL Research in Brain Metastases

Radiomics extracts high-dimensional quantitative data reflecting imaging phenotypes from tumor segmentation that aims to support clinical decision-making. Briefly, radiomic features include shape, first-order features, and second-order features; importantly, radiomics can often identify hidden information that is inaccessible to radiologists (7, 8).

DL is a subset of machine learning that is based around neural network structure. Unlike radiomics, which require predefined handcrafted features, DL is based on representation learning in which the algorithm automatically discovers the representations needed for object detection or classification from the provided data. Convolutional neural networks (CNN) are currently the most popular type of DL architecture in medical imaging; these networks consist of an input layer, hidden layers, and an output layer. Figure 1 shows schematic illustrations of radiomics and DL pipelines.

Briefly, DL is applied in tasks such as automatic detection, segmentation, or image synthesis, whereas both radiomics and DL can be applied in classification tasks. Current research representative of the state of radiomic and DL studies in brain metastases are summarized in Table 1. Representative research was based not only on performance, but also on the validation method (internal validation methods such as cross-validation or split train-test sets produce overly optimistic results (7), studies with external validation were preferred although performance was often lower), and pathologic confirmation methods (as it relates to determining the molecular status of brain metastases, research including molecular status that was determined from brain tissues themselves, rather than the primary tumor, was preferred). Figure 2 shows the original research regarding radiomics and DL in brain metastases according to the (a) published year and (b) research category. The PubMed MEDLINE database was used to search and collect all original research papers focusing on radiomics or DL published before January 15, 2021 using the following search terms: ("brain metastasis" OR "brain metastases") AND ("radiomic" or "deep learning" or "neural network" or "machine learning"). Articles which were not in field of interest or review articles were excluded.

Automatic Detection and Segmentation of Brain Metastases

Due to the unique characteristics of brain metastases as compared to other common brain tumors such as gliomas or meningiomas, automatic detection of brain metastases is challenging. Brain metastases may be substantially smaller than gliomas and often present at multiple sites; however, it is important to note that the detection of even subcentimeter lesions is crucial for choosing the correct treatment strategy, especially in case of SRS (8). Moreover, brain metastases near the leptomeningeal vessels may be missed or, conversely, leptomeningeal vessels may mimic metastases and be misidentified as such (9, 10). The segmentation of the brain metastases is also important for response assessment. Although the target lesions according to the Response Assessment in Neuro-Oncology Brain Metastases (RANO-BM) are currently determined using bidimensional measurements of contrast-enhancing lesions, the RANO-BM encourages the inclusion of volumetric response when feasible (11). However, manual detection and segmentation of brain metastases by radiologists or clinicians is not only laborious, but is also prone to error; interobserver variability in target volume delineation has been reported in SRS (12), and manual segmentation of all lesions is time-consuming. Thus, there is a strong unmet clinical need for processes that facilitate the automatic detection and segmentation of brain metastases that can be met with DL methods.

Various studies have used DL systems for the detection of brain metastases, most of which are nicely summarized in a recent meta-analysis (13). These studies have applied CNNs (14-19), fully convolutional networks (20), or single-shot detector models (21), with a pooled proportion of sensitivity and false-positive (FP) rate per patient of 90.1% (95% confidence interval 84-95%) and 10, respectively

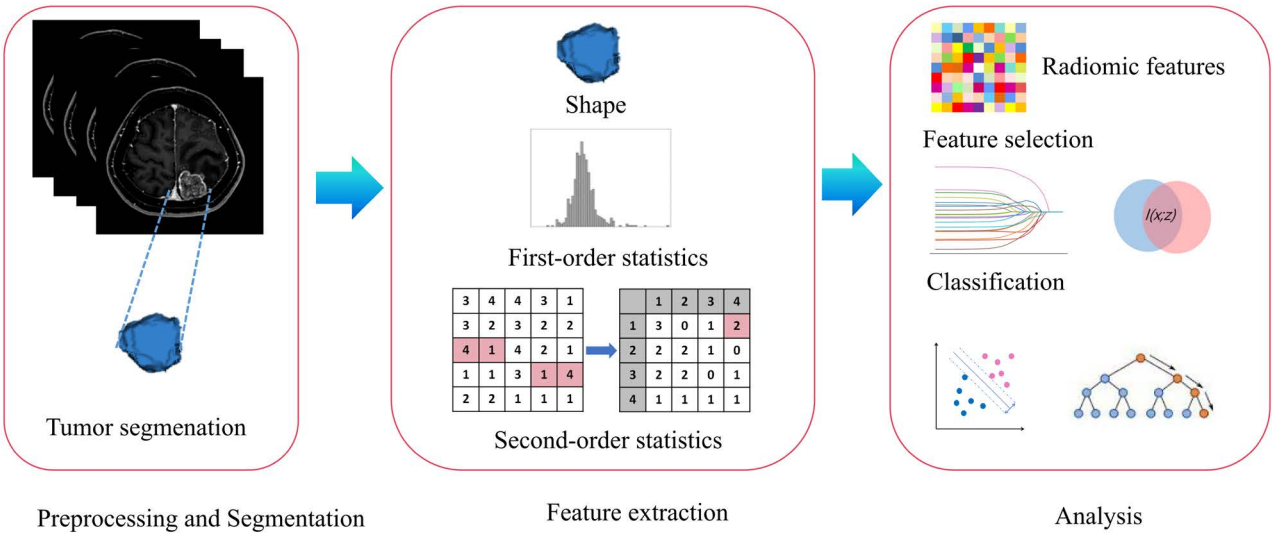

a

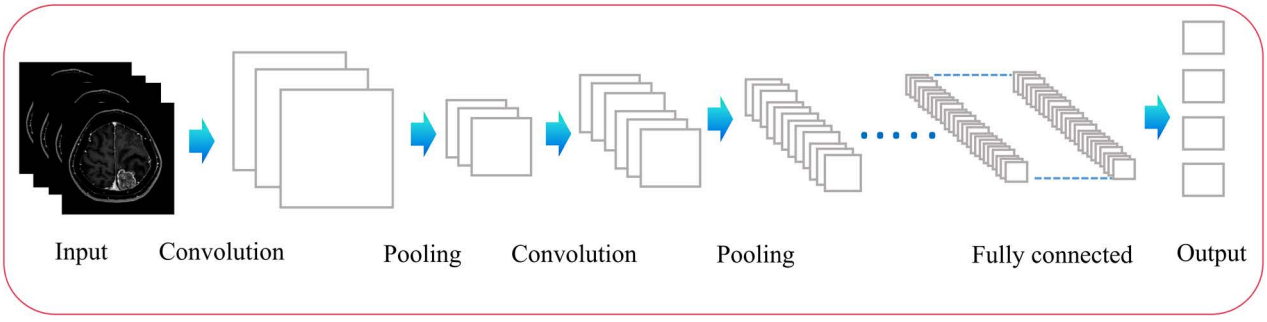

b

Fig. 1. Schematic illustration of radiomics and CNN pipelines. (a) In radiomics, tumor segmentation is performed after preprocessing. Radiomic features such as shape, first-order features, and second-order features are extracted. Feature selection and classification is then performed. (b) A CNN is composed of several different kinds of layers. A convolutional layer creates a feature map for pattern recognition of the image by applying a filter that scans the input image a few pixels at a time. A pooling layer scales down the amount of information the convolutional layer generated for each feature map and maintains the essential information. The process of convolution and pooling repeats several times. A fully connected layer applies weight over the input to predict an accurate label and generates final probabilities to determine a class for the image.

(13). Although these results are promising, DL research that performed subgroup analysis according to size showed poor performance in detecting small metastases; one study reported a sensitivity of 15% for identifying brain metastases < 3 mm (21), while another reported a sensitivity 50% for identifying lesions smaller than < 7 mm (16). The suboptimal performance of the DL models, especially with regard to small lesions, may hamper real-world integration of these models in clinical practice. Most of these studies implemented only contrast-enhanced three-dimensional (3D) gradient echo (GRE) images, which could be one cause of the low performance. A previous meta-analysis has shown that brain metastases can be more easily detected using contrast-enhanced spin-echo (SE) with or without black-blood (BB) imaging techniques than via GRE images, especially in cases with small lesions (< 5 mm) (22). A recent study implemented not only 3D GRE, but also 3D BB images and showed an overall sensitivity of 93.1%; for metastases < 3 mm, ≥ 3 mm and < 10 mm, and ≥ 10 mm, the sensitivities were 82.4%, 93.2%, and 100%, respectively (23). The FP per patient was 0.59 in the test, which is the lowest reported of any study to date. With the

Table 1. Current Research Representative of the State of Radiomics and DL Application in Brain Metastases

Topic	Methods	References	Data (train:test)	Outcomes	Test performance	External validation	Imaging modality
Automatic detection and/or segmentation	DL	Zhou et al. (21)	266 (212:54)	Brain metastases detection	Sensitivity = 81% FP/patient = 6	No	3D contrast-enhanced GRE
	DL	Xue et al. (20)	1652 (1487:165)	Brain metastases detection and segmentation	Sensitivity = 96% FP/patient = n/a Dice = 0.85 (calculated in lesions > 5 mm)	No	3D contrast-enhanced GRE
	DL	Park et al. (23)	282 (188:94)	Brain metastases detection and segmentation	Sensitivity = 93.1% FP/patient = 0.59 Dice = 0.82	No	3D contrast-enhanced GRE, 3D contrast-enhanced BB
Differential diagnosis	Radiomics	Bae et al. (36)	248 (166:82)	Single brain metastasis, glioblastoma	Overall AUC = 0.96	Yes	T2WI, 3D contrast-enhanced GRE
	DL	Shin et al. (37)	741 (598:143)	Single brain metastasis, glioblastoma	AUC = 0.835	Yes	T2WI, 3D contrast-enhanced GRE
Predicting origin	Radiomics	Kniep et al. (40)	189	Primary tumor type	AUCs = ranging from 0.64 (for NSCLC) to 0.82 (for melanoma)	No	Precontrast T1WI, FLAIR, 3D contrast-enhanced GRE or 3D BB
Predicting molecular marker	Radiomics	Park et al. (49)	51 (31:20)	EGFR mutation in NSCLC brain metastases	AUC = 0.73	No	DTI, 3D contrast-enhanced GRE
	Radiomics	Ahn et al. (48)	61 (189:21)†	EGFR mutation in NSCLC brain metastases	AUC = 0.87	No	Contrast-enhanced T1WI*
	Radiomics	Shofty et al. (52)	53	BRAF mutation in melanoma brain metastases	AUC = 0.78	No	3D contrast-enhanced T1WI*
Prognostication	Radiomics	Huang et al. (55)	161	PFS for NSCLC brain metastases treated with SRS	HR = 0.71 (PFS)	No	Contrast-enhanced SE
	Radiomics	Bhatia et al. (59)	105 (88:17)	OS for melanoma brain metastases receiving immune checkpoint inhibitors	HR = 0.68 (OS)	No	Contrast-enhanced T1WI*
Radiation necrosis vs. progression	Radiomics	Peng et al. (66)	82	Radiation necrosis	AUC = 0.81	No	FLAIR, contrast-enhanced T1WI
	Radiomics	Lohmann et al. (62)	52	Radiation necrosis	AUC = 0.96	No	Contrast-enhanced T1WI*, FET PET
	Radiomics	Hotta et al. (64)	41	Radiation necrosis (including patients from both brain metastases and gliomas)	AUC = 0.98	No	MET-PET
Treatment response assessment	Radiomics	Mouraviev et al. (73)	87	Local failure after SRS	AUC = 0.79	No	FLAIR, contrast-enhanced T1WI*
	Radiomics	Cha et al. (74)	110	Responder vs. nonresponder after SRS	AUC = 0.86	No	CT
Image synthesis	DL	Jun et al. (81)	75 (29:36)	Synthetic BB imaging	No significant difference in figure of merits between original BB and synthetic BB (0.94 vs. 0.97, P = 0.214)	No	3D contrast-enhanced GRE, 3D BB

AUC = area under the receiver operating curve; BB = black-blood; CT = computerized tomography; DL = deep learning; EGFR = epidermal growth factor receptor; FLAIR = fluid-attenuation inversion recovery; FP = false-positive; GRE = gradient echo; HR = hazard ration; MET = C11-methionine; n/a = not available; NSCLC = non-small cell lung cancer; OS = overall survival; PET = positron emission tomography; PFS = progression-free survival; SE = spin echo; SRS = stereotactic radiosurgery; T1WI = T1-weighted imaging. *GRE or BB not specified. †Indicating the number of brain metastases in the training and test set; the number of patients in the training and test set was not specified.

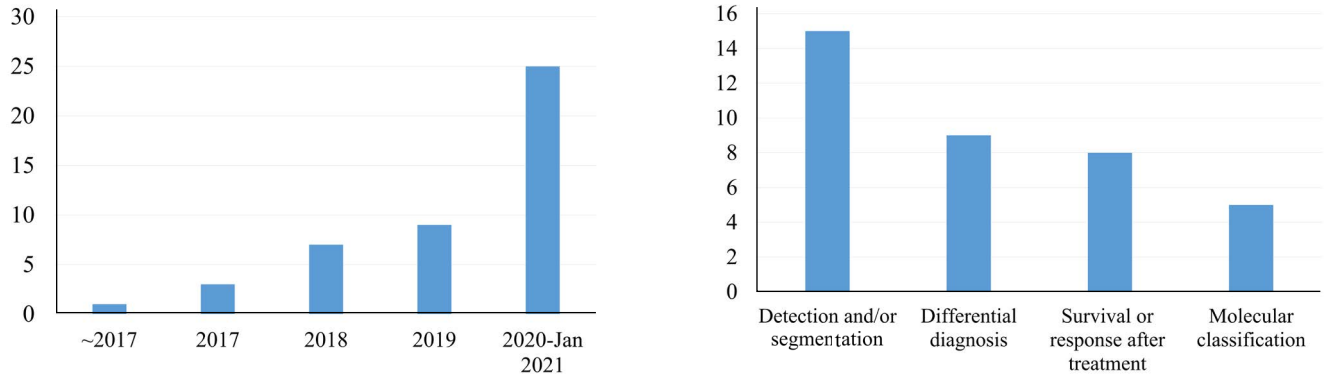

a b

Fig. 2. Graphs showing the number of published research articles regarding radiomics and DL in brain metastases in the PubMed database according to the year published (a) and the study category (b).

highest sensitivity for detecting small lesions, this study shows promise for future clinical applications. However, the research was performed from a single-institutional and relatively small dataset, which requires further external validation to prove its robustness. Moreover, 3D BB imaging has limitations because it is not technically feasible with all MRI instruments.

Several DL studies have performed segmentation along with automatic detection of brain metastases. Previous studies have reported Dice coefficients ranging from 0.77 (15), 0.79 (16), 0.82 (23), and 0.85 (20) in segmenting brain metastases. However, the study that reported the highest Dice coefficient, 0.85, did not included brain metastases smaller than 5 mm for this calculation (20); previous work has shown that smaller lesions are associated with lower Dice coefficients (24, 25). Nonetheless, these Dice coefficients are comparable to Dice coefficients from glioma automatic segmentation (26), and suggest that integration of segmentation information based on DL in the routine clinical practice may be feasible.

Differential Diagnosis

Differential Diagnosis with Glioblastoma

Brain metastases and glioblastoma are the most common malignant brain tumors in adults (27-29). In conventional MRI, differentiating single brain metastases from a glioblastoma by radiologists remains a challenge because both can manifest as a ring-enhancing mass with internal necrosis and peritumoral edema. Furthermore, up to 30% of brain metastases present as an initial manifestation of systemic malignancy (30) and approximately half present as a single lesion (1). This may cause diagnostic difficulties in differentiating between single brain metastases and glioblastomas.

To date, several radiomics studies have been performed to differentiate single brain metastases from glioblastoma. Majority of these studies were performed in a single institution with a split-sample validation method (31-35) save for one study which performed external validation, albeit using a smaller dataset (36). The latter study included segmentations from both contrast-enhancing and peritumoral edema on contrast-enhanced T1-weighted images (T1WI) and T2-weighted images (T2WI), and utilized deep neural network for classification, resulting in an area under receiver operating characteristic curve (AUC) of 0.96 in external validation (36). Considering the fact that the contrast-enhancing area and the peritumoral edema show different underlying pathophysiology in metastases and glioblastomas, implementation of both contrast-enhancing and peritumoral T2 hyperintense masks showed the highest diagnostic performance in the study as compared to DL using only a contrast-enhancing mask (AUC 0.89) or peritumoral T2 hyperintense mask (AUC 0.83), respectively. The radiomics model showed overall higher performance than radiologists (AUCs of 0.77 and 0.90, respectively).

One study performed DL based on ResNet-50 to differentiate single brain metastases from glioblastomas (37). Using contrast-enhanced T1WI and T2WI with rectangular regions of interest, the AUC of the DL model was 0.835 in external validation, which was higher than those of neuroradiologists (AUCs of 0.768 and 0.708, respectively).

Predicting the Origin of Brain Metastases

In 30% of patients with brain metastases, brain metastases may be diagnosed before primary tumor diagnosis (precocious presentation) or in conjunction with primary tumors (synchronous presentation) (38). Accurate identification of the primary tumor origin is crucial for treatment planning and prognosis predictions. Moreover, diagnostic decision making for patients with unknown primary tumor origin at the time of brain metastases diagnosis may require time-consuming testing, including chest/abdomen computerized tomography (CT), and positron emission tomography-CT (PET-CT). For these patients, advanced imaging-based tissue differentiation could contribute to more focused primary lesion detection, thereby accelerating therapy initiation.

In a feasibility study from a small single center dataset with nested cross-validation, 3D radiomic features from contrast-enhanced T1WIs showed promising results in differentiating the origin of brain metastases, with an overall AUC of 0.87 (39). In another study with a larger dataset from a single center which used 10-fold cross-validation, precontrast and contrast-enhanced T1WIs as well as fluid-attenuation inversion recovery (FLAIR) images were implemented. AUCs ranged between 0.64 (for non-small cell lung cancer) and 0.82 (for melanoma) (40). The prediction performance was superior to the classification performed by radiologists.

Prediction of Molecular Markers: towards "Virtual Biopsy"

Recent advances in targeted therapies have led to a paradigm shift in the diagnoses of patients with brain metastases. Figure 3 shows the genomic landscape of brain metastases according to primary tumor. For example, the use of next-generation systemic tyrosine kinase inhibitors (TKIs) for epidermal growth factor receptor (EGFR) in non-small cell lung cancer (NSCLC) showed greater intracranial activity than non-targeted local treatments against brain metastases from tumors with EGFR mutations (41). Gene expression analyses have identified distinct molecular subtypes of breast cancer (luminal A, luminal B, HER2 positive, and triple negative), each with unique metastatic patterns; patients with HER2-positive and triple-negative tumors are most likely to develop brain metastases (42). In melanomas, BRAF mutant tumors may undergo BRAF-targeted therapy with improved survival (43, 44).

One may ask why we should attempt to determine information about the molecular status of brain metastases, because in the majority of cases, the molecular markers are already obtained from the primary tumor. Excluding rare cases in which biopsy from the primary tumor is not feasible, obtaining noninvasive information about the molecular marker status of the brain metastases themselves may not seem necessary despite a dearth of evidence to the contrary. Neuroradiologists often fail to acknowledge the concept of "inter-tumoral heterogeneity" between the primary tumor and brain metastases. Recent studies have shown that primary tumors and brain metastases do not always share the same mutation status; in 53% of cases, there were alterations in the brain metastases that were not detected in the matched primary-tumor sample, while the spatially and temporally separated brain metastasis sites were genetically homogeneous (45). One of the mechanisms that has been proposed to explain the heterogeneity of primary tumors and brain metastases suggests that the metastatic lesion can arise through different genetic drafts or subclonal selections within the primary tumor (46). The molecular status of a minor population with acquired metastatic ability may result in discordance in the EGFR mutation status between primary and metastatic tumors. Figure 4 shows a model of primary intra-tumoral heterogeneity giving rise to brain metastases characterized by inter-tumor heterogeneity.

Although the European Association of Neuro-Oncology (EANO) recommends tissue diagnosis from brain metastases in order to evaluate the molecular marker status even when the markers have already been assessed from the extracranial tumor (47), biopsy is invasive and not feasible in many cases. The difficulty of routine brain biopsies promotes the integration of future "virtual biopsy" methods based on quantitative image analysis.

There have been several studies that aimed to predict the molecular status of brain metastases (48-52), and among these studies, two studies performed radiomics analysis of molecular information gathered directly from brain tissue (49). Most of the studies were performed to evaluate the EGFR mutation status of patients with lung cancer from a single institution (48-51), and a radiomics model using the FLAIR sequence yielded an AUC of 0.87 in the split-sample test set (51). The study that obtained the EGFR molecular status from pathologically confirmed brain tissue showed a lower performance with an AUC of 0.73 in the split-sample test set using diffusion tensor imaging and contrast-enhanced T1WI (49). Notably, the overall discordance rate between primary lung cancer and corresponding brain tumors among available patients was 12% (51). Another study additionally classified the anaplastic lymphoma kinase

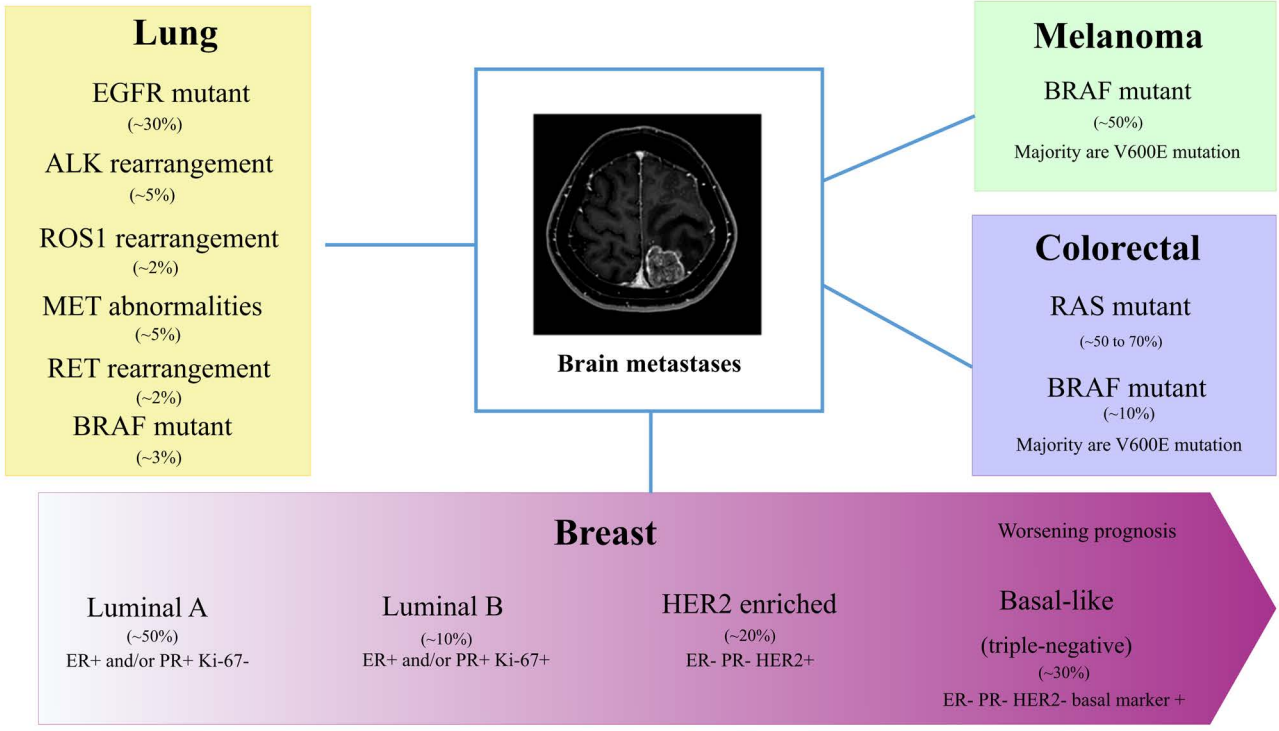

Fig. 3. Genomic landscape of brain metastases according to primary tumor. Because there was a scarcity of research in the imaging findings according to molecular markers, the radiogenomic landscape is not specified. Numbers in parenthesis indicate the percentage of molecular markers in the brain metastases itself, rather than the percentage in the primary tumor. ALK = anaplastic lymphoma kinase; EGFR = epidermal growth factor receptor; ER = estrogen receptor; HER2 = human epidermal growth factor receptor 2; PR = progesterone receptor

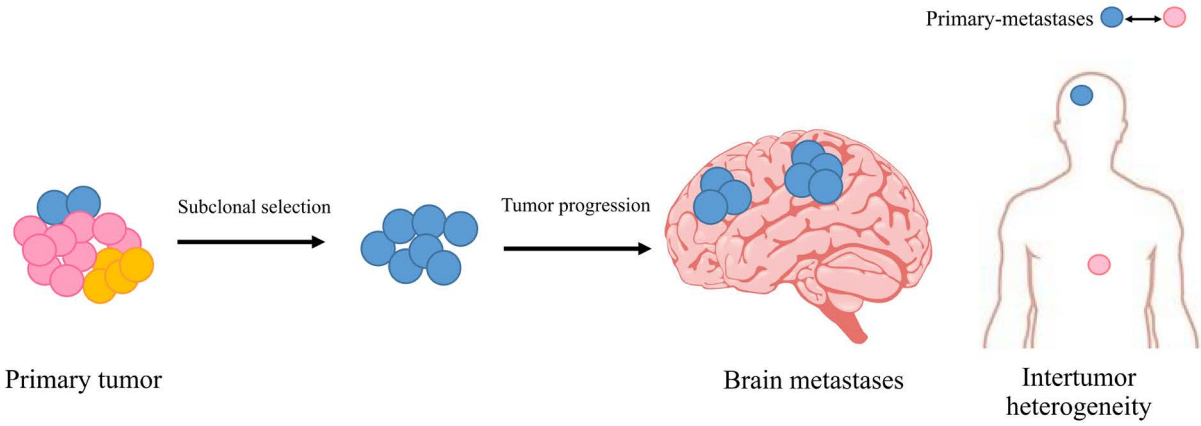

Fig. 4. Model of primary intra-tumoral heterogeneity giving rise to brain metastases characterized by inter-tumor heterogeneity.

(ALK) and KRAS (Kirsten rat sarcoma) mutation statuses from lung cancer and brain metastases using contrast-enhanced T1WI and FLAIR, with an AUC of 0.915 and 0.985, respectively, via leave-one-out cross-validation. On the other hand, another study that made predictions as to the BRAF mutation status in melanoma brain metastases from pathologically confirmed brain tissue using data from two institutions via contrast-enhanced T1WI reported an AUC of 0.78 in 5-fold cross-validation (52).

Prognostication

As mentioned in the introduction, the Graded Prognostic Assessment (GPA) (6) is the most prominent prognostic index, including the number of brain metastases as a prognostic factor in primary lung cancer, melanoma, and renal cell cancer. However, the number of brain metastases is rather simplistic information compared with the high-dimensional data available through imaging. Radiomic features and DL methods are not yet widely adopted in clinical prognostication models despite their enormous potential to capture underlying tumor biology and stratify outcomes.

SRS is a commonly used treatment strategy for patients with small brain metastases that has demonstrated improved local control and the ability to spare surrounding normal tissues (53). Nevertheless, when considering SRS, models such as GPA are predominantly analysed with overall survival (OS) and may be influenced by the competing risk of death as it relates to the systemic progression of disease. Moreover, predictions for therapeutic responsiveness vary substantially (54), promoting the development of more personalized models. Among radiomics studies that sought to predict progression-free survival (PFS) and/or OS in brain metastases treated with SRS, (55-57) the largest study was performed in 161 patients with NSCLC brain metastases in a single institution using contrast-enhanced T1WI (55). A multivariable cox proportional hazards model without any type of validation revealed that a higher zone percentage (HR = 0.71, P = 0.022) was independently associated with a longer PFS. The other two studies performed proof-of-concept radiomics studies on smaller datasets, in 48 patients (NSCLC and melanoma brain metastases) and 44 patients (breast cancer brain metastases), respectively (56, 57). The level of enhancing tumor volume was independently associated with a longer OS (HR = 0.38, P = 0.006) in the former study, whereas kurtosis was independently associated with a longer PFS (HR = 0.72, P = 0.008) in the latter study.

In melanoma brain metastases, immune checkpoint inhibitors such as cytotoxic T-lymphocyte antigen 4 (CTLA-4) inhibitors and programmed cell death protein 1 (PD-1) inhibitors have dramatically improved the prognosis and treatment of affected patients (58). However, clinical data show that there is heterogeneity in patient response to immune checkpoint inhibitors. A radiomics study was performed to predict OS in melanoma brain metastases treated with immune checkpoint inhibitors using contrast-enhanced T1WI (59). The mean Laplacian of Gaussian (LoG) feature showed significance in univariable analysis (HR = 0.68, P = 0.001), but not in multivariable analysis incorporating lactate dehydrogenase levels and performance status. The mean LoG was confirmed to be significant in an independent dataset.

Treatment-Related Change and Treatment Response

Differentiation of Radiation Injury from Tumor Progression

Aggressive treatment of brain metastases with SRS has improved the median survival time for affected patients considerably (60), however, radiation necrosis occurs in up to 34% of cases at 24 months after treatment and is associated with significant morbidity in 10-17% of cases (61). Radiation necrosis appears as an enhancing mass with surrounding edema on MRI and presents with severe neurologic disturbances that closely mimic tumor progression. Because tumor progression may require further treatment and radiation necrosis can be treated conservatively, the ability to distinguish the two after SRS in brain metastases is clinically important.

There are various studies differentiating recurrent metastases from radiation necrosis. Due to the difficulty of identifying radiation, in addition to conventional MRI, various imaging modalities, such as static O-(2-[^{18}F] fluoroethyl)-L-tyrosine (FET) PET or 11C-methionine PET-CT, have been applied in these models (62-64). One recent MRI based study used a "delta" radiomics model from both T2WI and contrast-enhanced T1WI, representing the changes in features from pretreatment to posttreatment MRI, with an AUC of 0.73 in leave-one-out cross-validation (65). Another study using FLAIR and contrast-enhanced T1WI reported an AUC of 0.81 in leave-one-out cross-validation (66). Among two different studies using FET-PET (62, 63), combined FET PET/CE-MRI radiomics showed an AUC of 0.79 in 10-fold cross-validation in one study, and showed higher performance than either modality alone (62). One study used 11C-methionine PET-CT to differentiate radiation necrosis from recurrent brain tumors (which included both brain metastases and gliomas). The AUC of the 10-fold cross-validated radiomics model was 0.98, which was higher than the AUC of 0.73 according to the tumor-to-normal cortex ratio (64).

Predicting Treatment Response in SRS

Randomized clinical trials have shown that SRS alone results in less neurocognitive dysfunction and a better quality of life than SRS plus WBRT without a significant

decrease in survival (67-70). Thus, SRS has emerged as a common treatment in patients with a limited number brain metastases (71), and EANO guidelines state that the absolute number of brain metastases is becoming less crucial in the choice to use SRS (47), further promoting its use. However, these trials have also demonstrated that SRS alone is associated with increased local failure as well as a higher rate of new, distant brain metastases than SRS plus WBRT (67, 68, 70). Notably, among the randomized trials, the one-year local failure rates ranged between 27-33% for SRS alone vs 0-11% for SRS plus WBRT (67, 68, 70). Thus, prediction of local failure in SRS may aid in treatment decision making; patients at high risk of local failure in SRS may benefit from additional treatments such as hippocampal-avoidance WBRT, which has shown comparable disease control to SRS while reducing the neurocognitive dysfunction of WBRT (72).

One study performed radiomics analysis to predict local failure per-lesion in brain metastases treated with SRS via MRI using contrast-enhanced T1WI and FLAIR, showing an AUC of 0.79 using leave-one-patient validation with a model combining radiomic and clinical features (73). Another study using CT radiomics demonstrated a CNN-based radiomics model with an AUC of 0.86 in a split-sample test set that generated accurate predictions of SRS response per-patient (74). In a study using 11C-methionine PET-CT in a small dataset, the radiomic features were extracted from a fully automatically segmented biological target volume; the radiomics model showed an AUC of 0.73 to predict SRS response per-patient via 5-fold cross-validation (75).

Differentiation of Pseudoprogression from Tumor Progression in Immunotherapy

In patients with brain metastases using immune checkpoint inhibitors, such as CTLA-4 inhibitors, PD-1 inhibitors, and programmed cell death protein ligand 1 (PD-L1) inhibitors, pseudoprogression is one of the most critical clinical and imaging challenges. Pseudoprogression is a tumor-related response to treatment that includes the intratumoral infiltration of cytotoxic T cells (CD8+) (76). A transient appearance of new contrast-enhancing lesions at either local or even distant sites can occur, and is defined as an objective tumor response after an initial increase in total tumor volume or the appearance of new lesions, even at distant sites (77). The immunotherapy Response Assessment in Neuro-Oncology (iRANO) criteria stipulates that early increases in lesion size and/or the development of new lesions within 6 months of immunotherapy does not define disease progression unless those changes are confirmed on follow-up MRI (78).

To date, there has been lack of radiomics or DL studies that attempt to differentiate pseudoprogression from tumor progression in brain metastases patients undergoing immunotherapy. In a recent study with metastatic melanoma patients (excluding brain metastases patients), a combined blood and PET-CT radiomics model showed an AUC of 0.82 in nested cross-validation for predicting pseudoprogression (79).

Image Synthesis

Considering the cost of scanning high-quality single modality images or homogeneous multimodality images, medical image synthesis methods have been extensively explored for clinical applications (80). To date, one study has focused on synthetic 3D BB imaging of brain metastases. Usually, in brain metastases protocols, 3D BB imaging is performed in addition to 3D GRE imaging, which requires additional scan time. Moreover, 3D BB imaging is not available from some MR vendors. Thus, the study has proposed a deep-learned 3D BB imaging method by which 3D CNN outputs based on 3D GRE imaging can be used for detecting brain metastases in a small institutional dataset (81). The figure of merits, which indicate the diagnostic performance of radiologists, were 0.97 with deep-learned BB and 0.94 with the original BB in a split-sample test set, suggesting that deep-learned BB imaging is highly comparable to the original BB imaging.

Another study, which was not performed in brain metastases but in glioma patients and healthy subjects, created virtual contrast enhancement from noncontrast multiparametric brain MRI with Bayesian DL (82). The virtual contrast enhancement imaging yielded a sensitivity and specificity of 91.8% and 91.2%, respectively, and a mean AUC, peak signal-to-noise ratio, and structural similarity index of 0.97, 22.97, and 0.87, respectively, via 10-fold cross-validation. Although virtual contrast imaging may seem to be more difficult or impossible in brain metastases imaging, which includes multiple and small lesions compared to the typically single mass to be identified in glioma imaging, it could be an interesting aspect to investigate.

Promises, Pitfalls, and Future Roadmap

Radiomics and DL, given their ability to discern patterns and combine information, show promise for the future

of radiology and precision medicine. An example of an ideal artificial intelligence-based system integrated into imaging protocols to improve treatment decisions in brain metastases is shown in Figure 5.

There is vast room for improvement in radiomics and DL as they related to the proper management of brain metastases. Despite the increasing number of publications, there are a relatively small number of studies performed in brain metastases compared to the many published that examine gliomas; this leaves a great deal of unexplored territory that could potentially yield substantial improvements in patient outcomes.

Forward Guidance

Currently, most research on brain metastases are technical feasibility studies without the true external validation required to prove robustness (13). For clinical translation of radiomics and DL studies, methodology standardization and quality improvements are necessary. Authors should move to investigate the performance of these models in real-world clinical settings and determine how they affect patient management rather than simply building and testing models. Currently, several guidance materials already exist (83, 84), and AI- and machine learning-specific guidelines to the STARD statement (STARD-AI) and TRIPOD statement (TRIPOD-ML) are being developed (85, 86).

Currently, as they relate to radiomics research, specific guidance materials such as the Image Biomarker Standardization Initiative (IBSI) (87) and radiomics quality score (RQS) list (88, 89) suggest mandatory steps for radiomics analyses.

Considerations Regarding MRI Application of Radiomics and DL

Real-world MRIs are acquired in different vendors, coils, acquisitions, and scanning protocols, leading to a heterogeneous dataset that could compromise the performance and reproducibility of radiomics and DL models. Moreover, conventional MRIs are acquired in arbitrary units, and different signal intensity normalization methods may

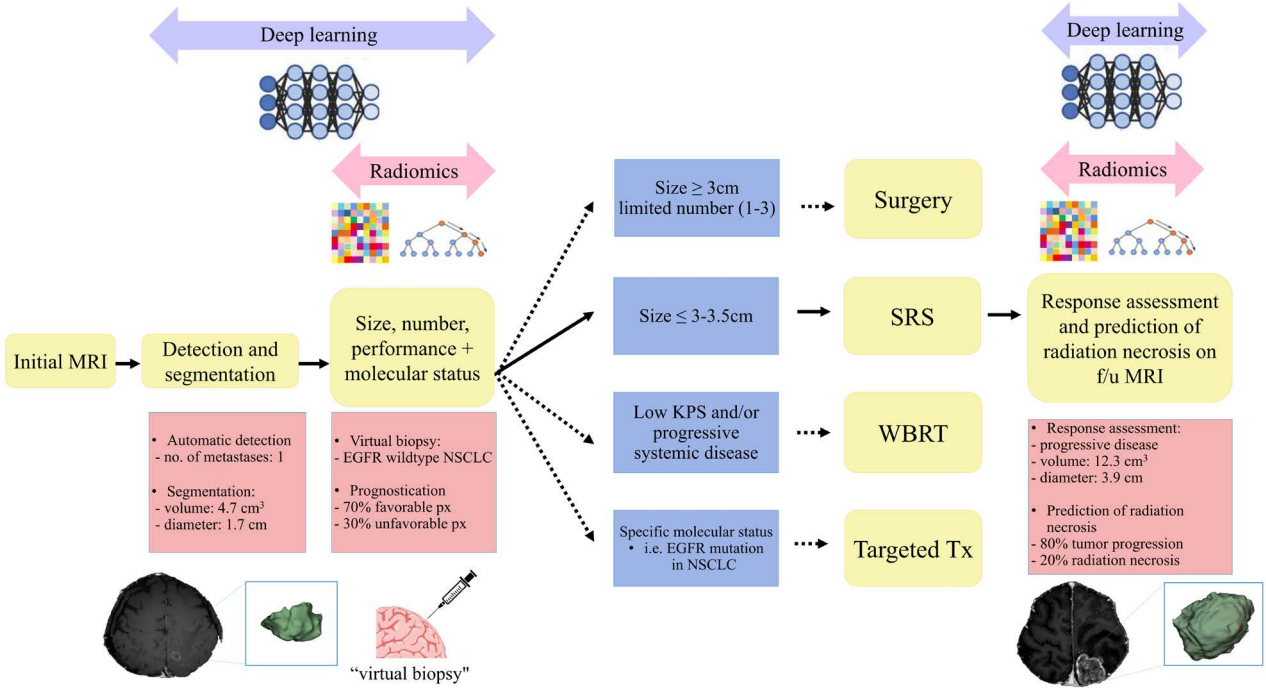

Fig. 5. Example of future radiomics- and deep learning-implemented brain metastases imaging and clinical management workflow in a EGFR-wildtype NSCLC brain metastasis. After initial imaging, automatic detection and segmentation would be performed, revealing the number and volumetric measurement of brain metastases. Virtual biopsy could then be performed predicting the molecular marker of the brain metastases separate from the primary tumor, and personalized prediction of survival could be performed by integrating all relevant clinical data. Optimal treatment could then be recommended (which is SRS in this example). On follow-up imaging, response assessments can be performed, and an analysis system could generate a probabilistic differential of tumor progression or radiation necrosis.

also affect overall performance (90). Although there is no golden rule for achieving multicenter reproducibility in radiomics and DL models, several ideas have been tested in clinical settings (91) and should be taken into consideration when planning future research.

Techniques to overcome Insufficient Data in Artificial Intelligence

One glaring limitation of radiomics and DL systems for the identification of brain metastases is the insufficient amount of data. This is especially true from a molecular biology perspective as there are a very limited number of cases in which molecular status was confirmed directly from brain tissue. 'Data-hungry' radiomics and DL methods may not be easily applied, and well-designed multi-institutional datasets are indicated.

Apart from larger multi-institutional datasets, many technical aspects can be applied to solve the problem of small datasets, such as transfer learning, meta-learning, or few-shot learning. Transfer learning is an alternative approach that uses pre-trained state-of-the-art CNN models, such as models trained from the ImageNet dataset, and is known to achieve a higher performance than those obtained by training CNNs from scratch (full-training) (92, 93). Meta-learning aims to improve the learning algorithm itself given a series of training tasks from other unrelated sets (94). Few-shot learning can be considered a type of meta-learning that classifies new data having seen only a few training examples, which may be useful in rare diseases (95). Also, especially in a small data regime, incorporating domain knowledge may improve the performance (96). Generative adversarial networks (GAN) can also solve the problem by increasing sample size via synthetic image generation (97). As GANs are vulnerable to so-called "adversarial attacks (perturbations of the input which do not affect human recognition but change the output of the classifier)", caution should be used when applying GAN generated data to CNN models (98).

From Supervised Learning to Unsupervised (or Semi-supervised) Learning in DL

Although the majority of DL research in brain metastases is based on CNNs trained using a type of "supervised learning" (which infers a function from labeled training data consisting of a set of training examples), we speculate that the research paradigm will gradually shift from "supervised learning" to "unsupervised (or semi-supervised) learning" (which learns patterns from unlabeled data). Thus, GANs, which are generative models for unsupervised learning, may perform many tasks such as image synthesis, reconstruction, segmentation, and classification of brain metastases effectively (99). These systems are likely to slowly be integrated into future radiomics and DL research.

Towards Explainability: Explainable Artificial Intelligence (XAI) in Radiomics and DL

Lastly, as future studies focus more heavily on the clinical application of radiomics and DL in brain metastases, the "black box" model, which generally provides no information about how neural networks arrive at their predictions, will not be suitable. Because such lack of transparency may be not acceptable by clinicians, the development of methods for visualizing, explaining, and interpreting radiomics and DL is required (100). Thus, we speculate that "explainable artificial intelligence (XAI)", such as Local Interpretable Model Explanation (LIME) (101) and SHapely Additive exPlanations (SHAP) (102) will be integrated with existing radiomics models, while grad-CAM (103) and Randomized Input Sampling for Explanation of Black-box Models (RISE) (104) will be integrated with DL models.

In conclusion, radiomics and DL are promising research areas likely to improve the diagnosis and treatment of brain metastases, and many studies, albeit the majority being proof-of concept or technical feasibility studies, show potential for future clinical implementation. For radiomics and DL to become valid clinical tools, their performance must be validated with clinical testing. It is crucial for neuroradiologists to understand current unmet clinical needs and appropriately investigate these powerful tools for use in clinical practice in the future.

Acknowledgments

This research received funding from the Basic Science Research Program through the National Research Foundation of Korea (NRF) funded by the Ministry of Science, Information and Communication Technologies & Future Planning (2020R1A2C1003886). This research was also supported by Basic Science Research Program through the National Research Foundation of Korea (NRF) funded by the Ministry of Education (2020R1I1A1A01071648). This study was financially supported by the Faculty Research Grant of Yonsei University College of Medicine (6-2020-0149).

REFERENCES

1. Nayak L, Lee EQ, Wen PY. Epidemiology of brain metastases. Curr Oncol Rep 2012;14:48-54
2. Loeffler JS, Patchell RA, Sawaya R. Metastatic brain cancer. In Davita VT, Hellman S, Rosenberg SA, eds. Cancer: principles and practice of oncology. Philadelphia: JP Lippincott, 1997:2523
3. Kondziolka D, Patel A, Lunsford LD, Kassam A, Flickinger JC. Stereotactic radiosurgery plus whole brain radiotherapy versus radiotherapy alone for patients with multiple brain metastases. Int J Radiat Oncol Biol Phys 1999;45:427-434
4. Patchell RA, Tibbs PA, Walsh JW, et al. A randomized trial of surgery in the treatment of single metastases to the brain. N Engl J Med 1990;322:494-500
5. Mehta MP, Rodrigus P, Terhaard CH, et al. Survival and neurologic outcomes in a randomized trial of motexafin gadolinium and whole-brain radiation therapy in brain metastases. J Clin Oncol 2003;21:2529-2536
6. Sperduto PW, Kased N, Roberge D, et al. Summary report on the graded prognostic assessment: an accurate and facile diagnosis-specific tool to estimate survival for patients with brain metastases. J Clin Oncol 2012;30:419-425
7. An C, Park YW, Ahn SS, Han K, Kim H, Lee S-K. Radiomics machine learning study with a small sample size: single random training-test set split may result in unreliable results. https://www.researchsquare.com/article/rs-105766/v2. Accessed June 9, 2021
8. Anzalone N, Essig M, Lee SK, et al. Optimizing contrast-enhanced magnetic resonance imaging characterization of brain metastases: relevance to stereotactic radiosurgery. Neurosurgery 2013;72:691-701
9. Nagao E, Yoshiura T, Hiwatashi A, et al. 3D turbo spin-echo sequence with motion-sensitized driven-equilibrium preparation for detection of brain metastases on 3T MR imaging. AJNR Am J Neuroradiol 2011;32:664-670
10. Park YW, Ahn SJ. Comparison of contrast-enhanced T2 FLAIR and 3D T1 black-blood fast spin-echo for detection of leptomeningeal metastases. Investig Magn Reson Imaging 2018;22:86-93
11. Lin NU, Lee EQ, Aoyama H, et al. Response assessment criteria for brain metastases: proposal from the RANO group. Lancet Oncol 2015;16:e270-278
12. Growcott S, Dembrey T, Patel R, Eaton D, Cameron A. Inter-observer variability in target volume delineations of benign and metastatic brain tumours for stereotactic radiosurgery: results of a national quality assurance programme. Clin Oncol (R Coll Radiol) 2020;32:13-25
13. Cho SJ, Sunwoo L, Baik SH, Bae YJ, Choi BS, Kim JH. Brain metastasis detection using machine learning: a systematic review and meta-analysis. Neuro Oncol 2021;23:214-225
14. Kamnitsas K, Ledig C, Newcombe VFJ, et al. Efficient multi-scale 3D CNN with fully connected CRF for accurate brain lesion segmentation. Med Image Anal 2017;36:61-78
15. Charron O, Lallement A, Jarnet D, Noblet V, Clavier JB, Meyer P. Automatic detection and segmentation of brain metastases on multimodal MR images with a deep convolutional neural network. Comput Biol Med 2018;95:43-54
16. Grovik E, Yi D, Iv M, Tong E, Rubin D, Zaharchuk G. Deep learning enables automatic detection and segmentation of brain metastases on multisequence MRI. J Magn Reson Imaging 2020;51:175-182
17. Zhang M, Young GS, Chen H, et al. Deep-learning detection of cancer metastases to the brain on MRI. J Magn Reson Imaging 2020;52:1227-1236
18. Bousabarah K, Ruge M, Brand JS, et al. Deep convolutional neural networks for automated segmentation of brain metastases trained on clinical data. Radiat Oncol 2020;15:87
19. Dikici E, Ryu JL, Demirer M, et al. Automated brain metastases detection framework for T1-weighted contrast-enhanced 3D MRI. IEEE J Biomed Health Inform 2020;24:2883-2893
20. Xue J, Wang B, Ming Y, et al. Deep learning-based detection and segmentation-assisted management of brain metastases. Neuro Oncol 2020;22:505-514
21. Zhou Z, Sanders JW, Johnson JM, et al. Computer-aided detection of brain metastases in T1-weighted MRI for stereotactic radiosurgery using deep learning single-shot detectors. Radiology 2020;295:407-415
22. Suh CH, Jung SC, Kim KW, Pyo J. The detectability of brain metastases using contrast-enhanced spin-echo or gradient-echo images: a systematic review and meta-analysis. J Neurooncol 2016;129:363-371
23. Park YW, Jun Y, Lee Y, et al. Robust performance of deep learning for automatic detection and segmentation of brain metastases using three-dimensional black-blood and three-dimensional gradient echo imaging. Eur Radiol 2021;31:6686-6695
24. Woo I, Lee A, Jung SC, et al. Fully automatic segmentation of acute ischemic lesions on diffusion-weighted imaging using convolutional neural networks: comparison with conventional algorithms. Korean J Radiol 2019;20:1275-1284
25. Xue Y, Farhat FG, Boukrina O, et al. A multi-path 2.5 dimensional convolutional neural network system for segmenting stroke lesions in brain MRI images. Neuroimage Clin 2020;25:102118

26. Isensee F, Kickingereder P, Wick W, Bendszus M, Maier-Hein KH. No new-net. International MICCAI Brainlesion Workshop, 2018:234-244
27. Ostrom QT, Cioffi G, Gittleman H, et al. CBTRUS statistical report: primary brain and other central nervous system tumors diagnosed in the United States in 2012-2016. Neuro Oncol 2019;21:v1-v100
28. Kim YE, Choi SH, Lee ST, et al. Differentiation between glioblastoma and primary central nervous system lymphoma using dynamic susceptibility contrast-enhanced perfusion MR imaging: comparison study of the manual versus semiautomatic segmentation method. Investig Magn Reson Imaging 2017;21:9-19
29. Kwon YW, Moon W-J, Park M, et al. Dynamic susceptibility contrast (DSC) perfusion MR in the prediction of long-term survival of glioblastomas (GBM): correlation with MGMT promoter methylation and 1p/19q deletions. Investig Magn Reson Imaging 2018;22:158-167
30. Cagney DN, Martin AM, Catalano PJ, et al. Incidence and prognosis of patients with brain metastases at diagnosis of systemic malignancy: a population-based study. Neuro Oncol 2017;19:1511-1521
31. Qian Z, Li Y, Wang Y, et al. Differentiation of glioblastoma from solitary brain metastases using radiomic machine-learning classifiers. Cancer Lett 2019;451:128-135
32. Dong F, Li Q, Jiang B, et al. Differentiation of supratentorial single brain metastasis and glioblastoma by using peri-enhancing oedema region-derived radiomic features and multiple classifiers. Eur Radiol 2020;30:3015-3022
33. Chen C, Ou X, Wang J, Guo W, Ma X. Radiomics-based machine learning in differentiation between glioblastoma and metastatic brain tumors. Front Oncol 2019;9:806
34. Artzi M, Bressler I, Ben Bashat D. Differentiation between glioblastoma, brain metastasis and subtypes using radiomics analysis. J Magn Reson Imaging 2019;50:519-528
35. Ortiz-Ramon R, Ruiz-Espana S, Molla-Olmos E, Moratal D. Glioblastomas and brain metastases differentiation following an MRI texture analysis-based radiomics approach. Phys Med 2020;76:44-54
36. Bae S, An C, Ahn SS, et al. Robust performance of deep learning for distinguishing glioblastoma from single brain metastasis using radiomic features: model development and validation. Sci Rep 2020;10:12110
37. Shin I, Kim H, Ahn SS, et al. Development and validation of a deep learning-based model to distinguish glioblastoma from solitary brain metastasis using conventional MR images. AJNR Am J Neuroradiol 2021;42:838-844
38. Hughes RAC, Brainin M, Gilhus NE. European handbook of neurological management. Wiley-Blackwell, 2008
39. Ortiz-Ramon R, Larroza A, Ruiz-Espana S, Arana E, Moratal D. Classifying brain metastases by their primary site of origin using a radiomics approach based on texture analysis: a feasibility study. Eur Radiol 2018;28:4514-4523
40. Kniep HC, Madesta F, Schneider T, et al. Radiomics of brain MRI: utility in prediction of metastatic tumor type. Radiology 2019;290:479-487
41. Ballard P, Yates JW, Yang Z, et al. Preclinical comparison of osimertinib with other EGFR-TKIs in EGFR-mutant NSCLC brain metastases models, and early evidence of clinical brain metastases activity. Clin Cancer Res 2016;22:5130-5140
42. Soffietti R, Ahluwalia M, Lin N, Ruda R. Management of brain metastases according to molecular subtypes. Nat Rev Neurol 2020;16:557-574
43. Long GV, Trefzer U, Davies MA, et al. Dabrafenib in patients with Val600Glu or Val600Lys BRAF-mutant melanoma metastatic to the brain (BREAK-MB): a multicentre, open-label, phase 2 trial. Lancet Oncol 2012;13:1087-1095
44. Sloot S, Chen YA, Zhao X, et al. Improved survival of patients with melanoma brain metastases in the era of targeted BRAF and immune checkpoint therapies. Cancer 2018;124:297-305
45. Brastianos PK, Carter SL, Santagata S, et al. Genomic characterization of brain metastases reveals branched evolution and potential therapeutic targets. Cancer Discov 2015;5:1164-1177
46. Alderton GK. Tumour evolution: epigenetic and genetic heterogeneity in metastasis. Nat Rev Cancer 2017;17:141
47. Soffietti R, Abacioglu U, Baumert B, et al. Diagnosis and treatment of brain metastases from solid tumors: guidelines from the European Association of Neuro-Oncology (EANO). Neuro Oncol 2017;19:162-174
48. Ahn SJ, Kwon H, Yang JJ, et al. Contrast-enhanced T1-weighted image radiomics of brain metastases may predict EGFR mutation status in primary lung cancer. Sci Rep 2020;10:8905
49. Park YW, An C, Lee J, et al. Diffusion tensor and postcontrast T1-weighted imaging radiomics to differentiate the epidermal growth factor receptor mutation status of brain metastases from non-small cell lung cancer. Neuroradiology 2021;63:343-352
50. Chen BT, Jin T, Ye N, et al. Radiomic prediction of mutation status based on MR imaging of lung cancer brain metastases. Magn Reson Imaging 2020;69:49-56
51. Wang G, Wang B, Wang Z, et al. Radiomics signature of brain metastasis: prediction of EGFR mutation status. Eur Radiol 2021;31:4538-4547
52. Shofty B, Artzi M, Shtrozberg S, et al. Virtual biopsy using MRI radiomics for prediction of BRAF status in melanoma

brain metastasis. Sci Rep 2020;10:6623
53. Graber JJ, Cobbs CS, Olson JJ. Congress of neurological surgeons systematic review and evidence-based guidelines on the use of stereotactic radiosurgery in the treatment of adults with metastatic brain tumors. Neurosurgery 2019;84:E168-E170
54. Jaboin JJ, Ferraro DJ, DeWees TA, et al. Survival following gamma knife radiosurgery for brain metastasis from breast cancer. Radiat Oncol 2013;8:131
55. Huang CY, Lee CC, Yang HC, et al. Radiomics as prognostic factor in brain metastases treated with Gamma Knife radiosurgery. J Neurooncol 2020;146:439-449
56. Zheng Y, Geng D, Yu T, et al. Prognostic value of pretreatment MRI texture features in breast cancer brain metastasis treated with Gamma Knife radiosurgery. Acta Radiol 2021;62:1208-1216
57. Della Seta M, Collettini F, Chapiro J, et al. A 3D quantitative imaging biomarker in pre-treatment MRI predicts overall survival after stereotactic radiation therapy of patients with a singular brain metastasis. Acta Radiol 2019;60:1496-1503
58. Tawbi HA, Forsyth PA, Algazi A, et al. Combined nivolumab and ipilimumab in melanoma metastatic to the brain. N Engl J Med 2018;379:722-730
59. Bhatia A, Birger M, Veeraraghavan H, et al. MRI radiomic features are associated with survival in melanoma brain metastases treated with immune checkpoint inhibitors. Neuro Oncol 2019;21:1578-1586
60. Brown PD, Brown CA, Pollock BE, Gorman DA, Foote RL. Stereotactic radiosurgery for patients with "radioresistant" brain metastases. Neurosurgery 2002;51:656-665; discussion 665-657
61. Le Rhun E, Dhermain F, Vogin G, Reyns N, Metellus P. Radionecrosis after stereotactic radiotherapy for brain metastases. Expert Rev Neurother 2016;16:903-914
62. Lohmann P, Kocher M, Ceccon G, et al. Combined FET PET/MRI radiomics differentiates radiation injury from recurrent brain metastasis. Neuroimage Clin 2018;20:537-542
63. Lohmann P, Stoffels G, Ceccon G, et al. Radiation injury vs. recurrent brain metastasis: combining textural feature radiomics analysis and standard parameters may increase (18)F-FET PET accuracy without dynamic scans. Eur Radiol 2017;27:2916-2927
64. Hotta M, Minamimoto R, Miwa K. 11C-methionine-PET for differentiating recurrent brain tumor from radiation necrosis: radiomics approach with random forest classifier. Sci Rep 2019;9:15666
65. Zhang Z, Yang J, Ho A, et al. A predictive model for distinguishing radiation necrosis from tumour progression after gamma knife radiosurgery based on radiomic features from MR images. Eur Radiol 2018;28:2255-2263
66. Peng L, Parekh V, Huang P, et al. Distinguishing true progression from radionecrosis after stereotactic radiation therapy for brain metastases with machine learning and radiomics. Int J Radiat Oncol Biol Phys 2018;102:1236-1243
67. Aoyama H, Shirato H, Tago M, et al. Stereotactic radiosurgery plus whole-brain radiation therapy vs stereotactic radiosurgery alone for treatment of brain metastases: a randomized controlled trial. JAMA 2006;295:2483-2491
68. Chang EL, Wefel JS, Hess KR, et al. Neurocognition in patients with brain metastases treated with radiosurgery or radiosurgery plus whole-brain irradiation: a randomised controlled trial. Lancet Oncol 2009;10:1037-1044
69. Kocher M, Soffietti R, Abacioglu U, et al. Adjuvant whole-brain radiotherapy versus observation after radiosurgery or surgical resection of one to three cerebral metastases: results of the EORTC 22952-26001 study. J Clin Oncol 2011;29:134-141
70. Brown PD, Jaeckle K, Ballman KV, et al. Effect of radiosurgery alone vs radiosurgery with whole brain radiation therapy on cognitive function in patients with 1 to 3 brain metastases: a randomized clinical trial. JAMA 2016;316:401-409
71. Arvold ND, Lee EQ, Mehta MP, et al. Updates in the management of brain metastases. Neuro Oncol 2016;18:1043-1065
72. Gondi V, Pugh SL, Tome WA, et al. Preservation of memory with conformal avoidance of the hippocampal neural stem-cell compartment during whole-brain radiotherapy for brain metastases (RTOG 0933): a phase II multi-institutional trial. J Clin Oncol 2014;32:3810-3816
73. Mouraviev A, Detsky J, Sahgal A, et al. Use of radiomics for the prediction of local control of brain metastases after stereotactic radiosurgery. Neuro Oncol 2020;22:797-805
74. Cha YJ, Jang WI, Kim MS, et al. Prediction of response to stereotactic radiosurgery for brain metastases using convolutional neural networks. Anticancer Res 2018;38:5437-5445
75. Stefano A, Comelli A, Bravata V, et al. A preliminary PET radiomics study of brain metastases using a fully automatic segmentation method. BMC Bioinformatics 2020;21:325
76. Okada H, Kalinski P, Ueda R, et al. Induction of CD8+ T-cell responses against novel glioma-associated antigen peptides and clinical activity by vaccinations with {alpha}-type 1 polarized dendritic cells and polyinosinic-polycytidylic acid stabilized by lysine and carboxymethylcellulose in patients with recurrent malignant glioma. J Clin Oncol 2011;29:330-336

77. Nishino M, Hatabu H, Hodi FS. Imaging of cancer immunotherapy: current approaches and future directions. Radiology 2019;290:9-22
78. Okada H, Weller M, Huang R, et al. Immunotherapy response assessment in neuro-oncology: a report of the RANO working group. Lancet Oncol 2015;16:e534-e542
79. Basler L, Gabrys HS, Hogan SA, et al. Radiomics, tumor volume, and blood biomarkers for early prediction of pseudoprogression in patients with metastatic melanoma treated with immune checkpoint inhibition. Clin Cancer Res 2020;26:4414-4425
80. Yu B, Wang Y, Wang L, Shen D, Zhou L. Medical image synthesis via deep learning. Adv Exp Med Biol 2020;1213:23-44.
81. Jun Y, Eo T, Kim T, et al. Deep-learned 3D black-blood imaging using automatic labelling technique and 3D convolutional neural networks for detecting metastatic brain tumors. Sci Rep 2018;8:9450
82. Kleesiek J, Morshuis JN, Isensee F, et al. Can virtual contrast enhancement in brain MRI replace gadolinium?: a feasibility study. Invest Radiol 2019;54:653-660
83. England JR, Cheng PM. Artificial intelligence for medical image analysis: a guide for authors and reviewers. AJR Am J Roentgenol 2019;212:513-519
84. Bluemke DA, Moy L, Bredella MA, et al. Assessing radiology research on artificial intelligence: a brief guide for authors, reviewers, and readers-from the Radiology Editorial Board. Radiology 2020;294:487-489
85. Sounderajah V, Ashrafian H, Aggarwal R, et al. Developing specific reporting guidelines for diagnostic accuracy studies assessing AI interventions: the STARD-AI Steering Group. Nat Med 2020;26:807-808
86. Collins GS, Moons KGM. Reporting of artificial intelligence prediction models. Lancet 2019;393:1577-1579
87. Zwanenburg A, Vallieres M, Abdalah MA, et al. The image biomarker standardization initiative: standardized quantitative radiomics for high-throughput image-based phenotyping. Radiology 2020;295:328-338
88. Park JE, Kim D, Kim HS, et al. Quality of science and reporting of radiomics in oncologic studies: room for improvement according to radiomics quality score and TRIPOD statement. Eur Radiol 2020;30:523-536
89. Won SY, Park YW, Park M, Ahn SS, Kim J, Lee SK. Quality reporting of radiomics analysis in mild cognitive impairment and Alzheimer's disease: a roadmap for moving forward. Korean J Radiol 2020;21:1345-1354
90. Carre A, Klausner G, Edjlali M, et al. Standardization of brain MR images across machines and protocols: bridging the gap for MRI-based radiomics. Sci Rep 2020;10:12340
91. Park JE, Park SY, Kim HJ, Kim HS. Reproducibility and generalizability in radiomics modeling: possible strategies in radiologic and statistical perspectives. Korean J Radiol 2019;20:1124-1137
92. Shin HC, Roth HR, Gao M, et al. Deep convolutional neural networks for computer-aided detection: CNN architectures, dataset characteristics and transfer learning. IEEE Trans Med Imaging 2016;35:1285-1298
93. Sharma S, Mehra R. Breast cancer histology images classification: training from scratch or transfer learning? ICT Express 2018;4:247-254
94. Nichol A, Achiam J, Schulman J. On first-order meta-learning algorithms. arXiv preprint arXiv:1803.02999, 2018
95. Sun Q, Liu Y, Chua T-S, Schiele B. Meta-transfer learning for few-shot learning. Proceedings of the IEEE Conference on Computer Vision and Pattern Recognition (CVPR), 2019:403-412
96. Dalca AV, Guttag J, Sabuncu MR. Anatomical priors in convolutional networks for unsupervised biomedical segmentation. Proceedings of the IEEE Conference on Computer Vision and Pattern Recognition 2018:9290-9299
97. Han C, Hayashi H, Rundo L, et al. GAN-based synthetic brain MR image generation. 2018 IEEE 15th International Symposium on Biomedical Imaging (ISBI 2018) 2018:734-738
98. Samangouei P, Kabkab M, Chellappa R. Defense-gan: protecting classifiers against adversarial attacks using generative models. arXiv preprint arXiv:1805.06605 2018
99. Yi X, Walia E, Babyn P. Generative adversarial network in medical imaging: a review. Med Image Anal 2019;58:101552
100. Samek W, Müller K-R. Towards explainable artificial intelligence. In Samek W, Montavon G, Vedaldi A, Hansen LK, Müller K-R, eds. Explainable AI: interpreting, explaining and visualizing deep learning. Springer Nature, 2019:5-22
101. Mishra S, Sturm BL, Dixon S. Local interpretable model-agnostic explanations for music content analysis. ISMIR 2017:537-543
102. Lundberg S, Lee S-I. A unified approach to interpreting model predictions. arXiv preprint arXiv:1705.07874, 2017
103. Selvaraju RR, Das A, Vedantam R, Cogswell M, Parikh D, Batra D. Grad-cam: Why did you say that? arXiv preprint arXiv:1611.07450, 2016
104. Petsiuk V, Das A, Saenko K. Rise: randomized input sampling for explanation of black-box models. arXiv preprint arXiv:1806.07421, 2018